EUROPEAN ORGANIZATION FOR NUCLEAR RESEARCH

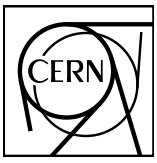

CERN-EP-2018-XXX
Day Month 2018

Scattering studies with low-energy kaon-proton femtoscopy in proton–proton collisions at the LHC

ALICE Collaboration*

Abstract

The study of the strength and behaviour of the antikaon-nucleon ($\overline{\mathrm{K}}\mathrm{N}$) interaction constitutes one of the key focuses of the strangeness sector in the low-energy Quantum Chromodynamics (QCD). In this letter a unique high-precision measurement of the strong interaction between kaons and protons, close and above the kinematic threshold, is presented. The femtoscopic measurements of the correlation function at low pair-frame relative momentum of ($\mathrm{K}^{+}\mathrm{p} \oplus \mathrm{K}^{-}\overline{\mathrm{p}}$) and ($\mathrm{K}^{-}\mathrm{p} \oplus \mathrm{K}^{+}\overline{\mathrm{p}}$) pairs measured in pp collisions at $\sqrt{s}$ = 5, 7 and 13 TeV are reported. A structure observed around a relative momentum of 58 MeV/c in the measured correlation function of ($\mathrm{K}^{-}\mathrm{p} \oplus \mathrm{K}^{+}\overline{\mathrm{p}}$) constitutes the first experimental observation of the opening of the ($\overline{\mathrm{K}}^{0}\mathrm{n} \oplus \mathrm{K}^{0}\overline{\mathrm{n}}$) isospin breaking channel due to the mass difference between charged and neutral kaons. The measured correlation functions have been compared to several models. The high-precision data at low relative momenta presented in this work prove femtoscopy to be a powerful complementary tool to scattering experiments and provide new constraints above the $\overline{\mathrm{K}}\mathrm{N}$ threshold for low-energy QCD chiral models.

*See Appendix A for the list of collaboration members

Scattering data of low-energy charged kaons with proton or deuteron targets are scarce. Only measurements performed decades ago in bubble chamber experiments or with emulsions exist for kaon incident momentum $p_{\rm lab}$ below 350 MeV/c [1–5]. Such data are essential to assess the low-energy cross-section of the interaction of kaons with protons and neutrons.

The K^+ and K^- behavior in the scattering process is very different and markedly depends on the meson strangeness content. The $\mathrm{K}^+\mathrm{N}$ interaction is well established [6], and it is characterized by a moderate repulsive potential, due to the strong and the Coulomb interactions. The $\mathrm{K}^+\mathrm{N}$ data can be employed to assess the strangeness content of the nucleon through the Sigma-term evaluation [7, 8] that can be extracted by the analytic continuation of the KN scattering amplitude by means of dispersion relations. The $\mathrm{K}^+\mathrm{p}$ scattering data alone can be used to thoroughly study the isovector part ($\mathrm{I} = 1$) of the KN scattering amplitude, while the isoscalar part ($\mathrm{I} = 0$) can be extracted by using the $\mathrm{K}^+\mathrm{d}$ data in combination.

Kaons with strangeness $\mathrm{S} = -1$ are strongly absorbed in the scattering process. The strength of the attractive $\overline{\mathrm{K}}\mathrm{N}$ interaction leads to the appearance of baryonic resonances, both with isospin $\mathrm{I} = 0$ and $\mathrm{I} = 1$, even below threshold, such as the $\Lambda(1405)$. This resonance in fact lies only 27 MeV/c^2 below the $\overline{\mathrm{K}}\mathrm{N}$ threshold and the general interpretation of its nature as a molecular state with two poles coupled to the $\overline{\mathrm{K}}\mathrm{N}$ and $\Sigma\pi$ channels [9–11] is widely accepted. However at present different theoretical approaches [12–21] predict a similar behavior above the $\overline{\mathrm{K}}\mathrm{N}$ threshold but large discrepancies arise in the subthreshold region due to the lack of precise constraints from experimental data. Experimental constraints on the $\overline{\mathrm{K}}\mathrm{N}$ interaction are fundamental for such models in order to reproduce the line shape of the resonance produced by different mechanisms and observed in different decay channels [22–26].

In the region above the threshold, experimental input was provided so far by available scattering data [1–5], which however are rather imprecise, and in particular absent in most of the inelastic channels for $p_{\rm lab}$ below 100 MeV/c, thus imposing weak constraints to models. Currently, the measurement of kaonic hydrogen [27] constitutes the most precise constraint at threshold and additional constraints come from studies of the formation of kaonic bound states [28–30]. Recently, the femtoscopy technique [31, 32], which measures the correlation of particle pairs at low relative momentum, has proven to be a powerful complementary tool to scattering experiments by providing high precision data on different baryon–baryon pairs [33–35], indicating a great sensitivity to the underlying strong potential in particular in the low relative momentum range.

For the $\overline{\mathrm{K}}\mathrm{N}$ system, in this low momentum regime, the $\overline{\mathrm{K}}^0\mathrm{n}$ isospin breaking channel due to the mass difference between K^- and $\overline{\mathrm{K}}^0$ is predicted to open up at $p_{\rm lab} = 89$ MeV/c but it has not yet been experimentally observed due to the difficulties in reaching such low energies with kaon beams. Precise data at such low momenta on the $\overline{\mathrm{K}}\mathrm{N}$ system are strongly needed to add additional constraints which, along with the results at threshold from kaonic atoms, can be used as an input for models to obtain precise extrapolations of the scattering amplitude in the sub-threshold region. The femtoscopic technique applied to Kp pairs delivers such data with precise measurements down to zero relative momentum.

In this letter, the momentum correlations of Kp pairs (($\mathrm{K}^+\mathrm{p} \oplus \mathrm{K}^-\overline{\mathrm{p}}$) and ($\mathrm{K}^-\mathrm{p} \oplus \mathrm{K}^+\overline{\mathrm{p}}$)) using the two-particle correlation function in pp collisions at different collision energies are presented. The same-charge pairs ($\mathrm{K}^+\mathrm{p} \oplus \mathrm{K}^-\overline{\mathrm{p}}$), because of the well described interaction and the lack of coupled-channel effects, are used as a benchmark to test the sensitivity of the correlation function to the strong interaction. The analysis presented here is based on minimum bias triggered pp collisions collected by the ALICE experiment [36] at the LHC in 2010, 2015, 2016 and 2017 at three different collision energies ($\sqrt{s}$ = 5 TeV, 7 TeV, and 13 TeV). The correlation function $C(k^*)$ is measured as a function of the momentum difference of the pair $k^* = \frac{1}{2}(\vec{p}_1{}^* - \vec{p}_2{}^*)$, where $\vec{p}_1{}^*$ and $\vec{p}_2{}^*$ are the momenta of the two particles in the pair rest frame. It is defined as $C(k^*) = \mathcal{N}\, A(k^*)/B(k^*)$, where $A(k^*)$ is the measured distribution of pairs from the same event, $B(k^*)$ is the reference distribution of pairs from mixed events and $\mathcal{N}$ is a normalization parameter. The denominator, $B(k^*)$, is formed by mixing particles from one event with particles from a pool of other events with similar number of charged particles at mid-rapidity and V_z interval (ΔV_z = 2 cm), where V_z is the position of the primary vertex of the collision along the beam axis.

The normalization parameter $\mathcal{N}$ is chosen such that the mean value of the correlation function equals unity for $400 < k^* < 600$ MeV/c.

The main sub-detectors used in this analysis are: the V0 detectors [37], which are used as trigger detectors, the Inner Tracking System (ITS) [38], the Time Projection Chamber (TPC) [39] and the Time-of-Flight (TOF) detector [40]. The ITS, TPC and TOF are located inside a 0.5 T solenoidal magnetic field and are used to track and identify charged particles. In order to ensure a uniform acceptance at mid-rapidity, events were selected by requiring the V_z of the event to be within 10 cm from the center of the ALICE detector. The rejection of pile-up is performed by exploiting the innermost silicon detector (SPD, part of ITS) vertexing capabilities, following the same procedure described in [35, 41]. After the application of the event selection criteria, about 874 million, 374 million, and 1 billion minimum bias pp events were analyzed at $\sqrt{s}$ = 5 TeV, 7 TeV, and 13 TeV, respectively.

As recently proposed in [42], in order to reduce the contribution from the mini-jet background in pp collisions, the events were classified according to their transverse sphericity ($S_{\rm T}$) , an observable which is known to be correlated with the number of hard parton–parton interactions in each event [43]. An event with only one hard parton–parton interaction will in general produce a jet-like distribution that yields low sphericity, while an event with several independent hard parton–parton interactions can yield higher sphericity as each (mini-)jet axis is oriented randomly. In order to reduce the strong mini-jet background at low momenta, only events with $S_{\rm T}$, defined as in [42], larger than 0.7 were considered in this analysis. Charged particles were tracked using the ITS and TPC, then selected by requiring that each track is reconstructed from at least 70 out of the 159 possible space points in the TPC. Only tracks in the pseudorapidity region $|\eta| < 0.8$, where ALICE is able to perform full tracking and provide the particle identification information, were considered in this analysis. To reject the contribution from secondary particles from weak decays and from interactions with the material, and to select tracks originating from the collision vertex, the tracks were required to have a Distance of Closest Approach (DCA) to the primary vertex smaller than 1.0 cm, both in the transverse plane (DCA$_{xy}$) and along the longitudinal (DCA$_z$) direction. For the same reason, tracks with a kink topology in the TPC, indicating weak decays of charged pions and kaons, were discarded. The charged kaons and protons were identified in a wide transverse momentum ($p_{\rm T}$) interval ($0.15 < p_{\rm T} < 1.4$ GeV/c for kaons and $0.4 < p_{\rm T} < 3$ GeV/c for protons) using the information provided by the TPC and the TOF detectors. The deviation of the measured specific ionization energy loss (dE/dx) in the TPC from the Bethe-Bloch parametrization was required to be within three standard deviations ($\sigma_{\rm TPC}$). For kaons with $p_{\rm T} > 0.4$ GeV/c and protons with $p_{\rm T} > 0.8$ GeV/c, a similar method was applied for the particle identification using the TOF, where, on top of TPC selection, a selection based on a maximum three standard deviation difference ($\sigma_{\rm TOF}$) from the expected signal at a given momentum was applied. Tracks identified ambiguously as belonging to both a proton and a kaon, were discarded. In order to remove the large fraction of $\rm e^+e^-$ pairs that can affect the extraction of the correlation function of the opposite-charge pairs, a selection on the $p_{\rm T}$ of kaon and protons was applied: kaon candidates are excluded if $0.3 < p_{\rm T} < 0.4$ GeV/c, while proton candidates are excluded in the interval between $0.6 < p_{\rm T} < 0.8$ GeV/c. The effect of these selections on the correlation function was studied for the same-charge pairs and has been found to be negligible. The purity of the selected particle samples, determined by Monte Carlo simulations, is larger than 99% in the considered $p_{\rm T}$ intervals for all analyzed dataset. The track selections criteria are summarized in Table 1.

The systematic uncertainties of the measured $C(k^*)$ were evaluated for each k^* interval by varying event and track selection criteria. The event sample is varied by changing the selection on the V_z position from $\pm$ 10 cm to $\pm$ 7 cm and by varying the sphericity of the accepted events from $S_{\rm T} > 0.7$ to $S_{\rm T} > 0.6$ and $S_{\rm T} > 0.8$. Systematic uncertainties related to the track selection criteria were studied by varying the selection on the DCA$_{xy}$ distributions within the experimental resolution. To study systematic effects related to particle identification, the number of standard deviations around the energy loss expected for kaons and protons in the TPC and, similarly, for the time of flight in the TOF was modified from 3σ to 2σ. For each source, the systematic uncertainty was estimated as the root-mean-square (RMS) of

Table 1: Summary of track selection criteria

Selection variable	Value
$\|\eta\|$	< 0.8
Number of TPC clusters	≥ 70
DCA_{xy} to primary vertex	< 1 cm
DCA_z to primary vertex	< 1 cm
Tracks with kink topology	rejected
$K^+(K^-)$ transverse momentum p_T	$0.15 < p_T < 0.3$ GeV/c $0.4 < p_T < 1.4$ GeV/c
$p(\overline{p})$ transverse momentum p_T	$0.4 < p_T < 0.6$ GeV/c $0.8 < p_T < 3.0$ GeV/c
Particle identification	n-σ_{TPC} <3 for K with $p_T > 0.4$ and p with $p_T > 0.8$: n-σ_{TPC} <3 + n-σ_{TOF} <3

the deviations. The total systematic uncertainty was calculated as the quadratic sum of each source's contribution and amounts to about 3% in the considered k^* intervals.

The measured correlation functions for $(K^+p \oplus K^-\overline{p})$ and $(K^-p \oplus K^+\overline{p})$ are shown in the upper panels of Fig. 1 and Fig. 2.

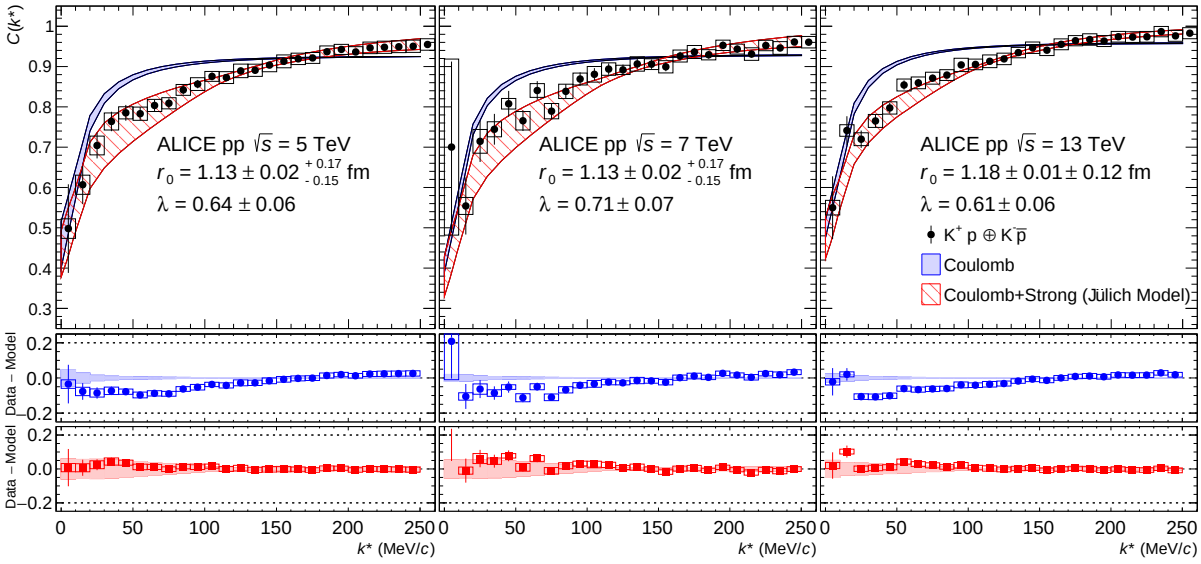

Fig. 1: (Color online)$(K^+p \oplus K^-\overline{p})$ correlation functions obtained from pp collisions at $\sqrt{s} = 5$ TeV (left), 7 TeV (middle) and 13 TeV (right) fitted with Eq. 1 including only a Coulomb interaction (blue) or in addition the strong interaction implemented in the Jülich model (red). The measurement is shown by the black markers, the vertical lines and the boxes represent the statistical and systematic uncertainties respectively. In the bottom panels of the figure, the difference between the data and models are shown. The bands represent the systematic uncertainty related to the determination of the λ parameter and to the source radius.

In both figures, each panel corresponds to a different collision energy, as indicated in the legend. The structure that can be seen in the $(K^-p \oplus K^+\overline{p})$ correlation function at k^* around 240 MeV/c in Fig. 2 is consistent with the $\Lambda(1520)$ which decays into K^-p, with a center-of-mass momentum for the particle pair of 243 MeV/c [51]. The correlation function of $(K^-p \oplus K^+\overline{p})$ exhibits also a structure between 50 and 60 MeV/c for the three collision energies. The k^* position of the structure is consistent with the

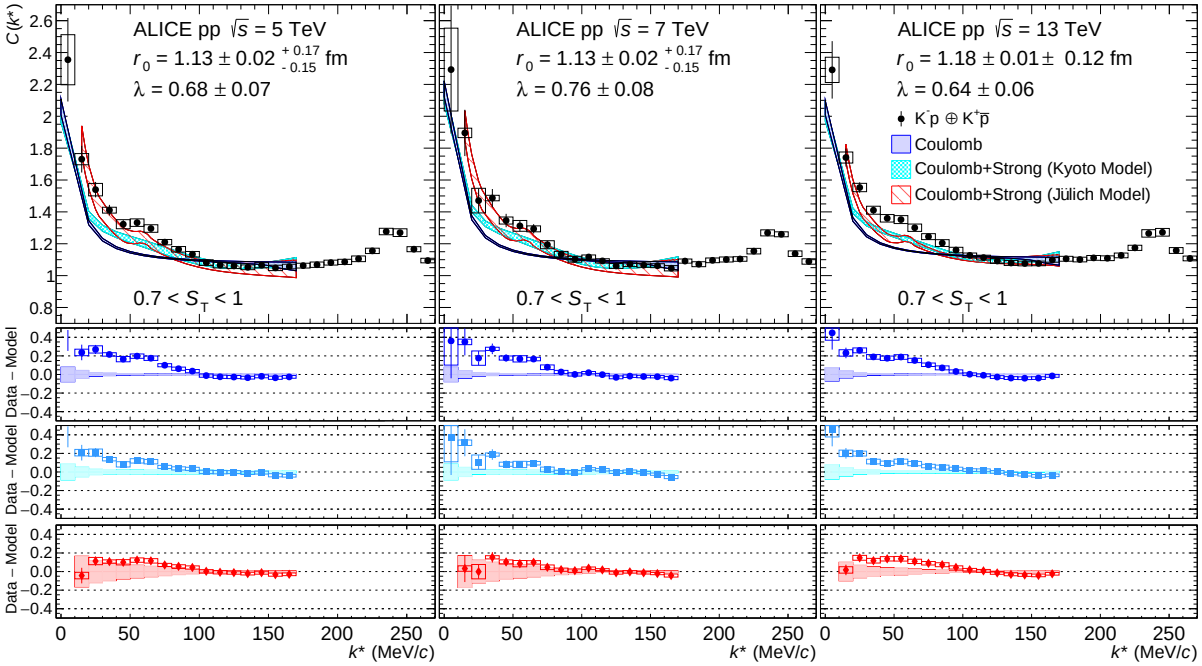

Fig. 2: (Color online)($K^-p \oplus K^+\bar{p}$) correlation functions obtained from pp collisions at $\sqrt{s}$ = 5 TeV (left), 7 TeV (middle) and 13 TeV (right) fitted with Eq. 1. The measurement is presented by the black markers, the vertical lines and the boxes represent the statistical and systematic uncertainties respectively. Three different potentials were considered: Coulomb potential (blue band), Kyoto model [44–48] (light blue band), Jülich model [49] where the physics masses of K^- and $\overline{K}^0$ are used [50] with the Coulomb interaction included (red band). In the bottom panels, differences between data and model are shown. The bands represent the systematic uncertainty related to the determination of the λ parameter and to the source radius.

threshold of the $\overline{K}^0 n$ ($K^0\bar{n}$) channel at $p_{\rm lab}$ = 89 MeV/c [52] which corresponds to k^* = 58 MeV/c. In order to quantify the significance of the observed structure, and since the three measured distributions are mutually compatible, the $C(k^*)$ measured at the three different energies were summed using the number of events for each data sample as a weight. The resulting $C(k^*)$ was interpolated with a spline considering the statistical uncertainties and the derivative of the spline was then evaluated. A change in the slope of the derivative consistent with a cusp effect in the k^* region between 50 and 60 MeV/c at the level of 4.4σ has been observed, to be compared with a significance of 30σ for $\Lambda(1520)$. The measurement presented in this letter is therefore the first experimental observation of the opening of the $\overline{K}^0 n$ ($K^0\bar{n}$) isospin breaking channel, showing that the femtoscopy technique is a unique tool to study the $\overline{K}p$ scattering, where the conventional scattering experiments at fixed target are difficult to perform.

The experimental correlation functions were also used to test different potentials to describe the interaction between K^+p ($K^-\bar{p}$) and K^-p ($K^+\bar{p}$). The measured correlation function $C(k^*)$ is compared with a theoretical function using the following equation

$$C(k^*) = N \cdot \left[1 + \lambda \cdot (C(k^*)^{theoretical} - 1)\right], \quad (1)$$

where the normalization N is a free parameter and λ represents the fraction of primary pairs in the sample multiplied by the purity of the sample. The λ parameter is fixed by fitting Monte Carlo (MC) templates to the experimental distributions of DCA_{xy} of kaons and protons, similarly to what is described in [35]. The model correlation function, $C(k^*)^{theoretical}$, is evaluated using the CATS framework [53].

The λ parameters obtained for each analyzed data sample are shown in each panel of Fig. 1 and Fig. 2 for same-charge and opposite-charge Kp pairs, and vary from 0.61 to 0.76 for each considered set. A systematic uncertainty of $\pm 10\%$ is associated with the λ parameters. This uncertainty was estimated by varying the Monte Carlo templates used in the feed-down estimation procedure based on PYTHIA 6 [54] for the analysis at $\sqrt{s}$ = 7 TeV and based on PYTHIA 8 [55] for the analyses performed at $\sqrt{s}$ = 5 TeV and 13 TeV, and varying the transport code used in the simulation from GEANT3 [56] to GEANT4 [57]. The theoretical correlation function $C(k^*)^{theoretical}$ depends not only on the interaction between particles, but also on the profile and the size of the particle emitting source. Under the assumption that there is a common Gaussian source for all particle pairs produced in pp collisions at a fixed energy, the size of the source considered in the present analysis is fixed from the baryon–baryon analyses described in [35] and [41]. On top of this, the impact of the decay of resonances (mainly K^* decaying into K and Δ decaying into p) on the determination of the radius was studied using different Monte Carlo simulations [54, 55] and found to be 10%. This contribution was linearly added to the systematic uncertainty associated with the radius. The radii of the considered Gaussian sources are $r_0 = 1.13 \pm 0.02^{+0.17}_{-0.15}$ fm [35] for collisions at $\sqrt{s}$ = 5 and 7 TeV, and $r_0 = 1.18 \pm 0.01 \pm 0.12$ fm [41] for the $\sqrt{s}$ = 13 TeV collisions.

The comparison of the measured $C(k^*)$ for same-charge Kp pairs with different models is shown in Fig. 1. Each panel presents the results at different collision energy and the comparison with two different scenarios: including only Coulomb repulsion and taking into account also the strong interaction. The blue band represents the correlation function evaluated as described in Eq. (1), assuming only the presence of the Coulomb potential to evaluate the $C(k^*)^{theoretical}$ term. Similarly, the red band represents the correlation function assuming the strong potential implemented in the Jülich model [58] in addition to the Coulomb potential. The latter has been implemented by correcting the wave function with the factor $\mathrm{e}^{i\delta_c}\sqrt{A_c(\eta)}$, where $\delta_c = \arg\Gamma(1+i\eta)$ is the Coulomb s-wave shift and $A_c(\eta) = 2\pi\eta\left(\mathrm{e}^{2\pi\eta}-1\right)^{-1}$ is the Gamow factor [59]. The factor η, in natural units, is given by $\alpha\mu z_1 z_2/k^*$, where α is the fine structure constant, $z_{1,2}$ the particles charge and μ their reduced mass. In the bottom panels, the difference between data and model for the three considered collision energies are shown. The width of the bands represents the range of uncertainties associated with the determination of the λ parameter and with the radius of the source. This comparison reveals that the Coulomb interaction is not able to describe the data points, while the introduction of a strong potential allows to reproduce consistently the data. Hence, the measured correlation functions are sensitive to the strong interaction and can be used to test different strong potentials for the $\mathrm{K}^-\mathrm{p}$ system.

The correlation functions obtained as a function of k^* for opposite-charge kaon–proton pairs are shown in Fig 2. As before, the measured $C(k^*)$ is reported for the three different collision energies and the $C(k^*)$ distributions were compared with different interaction models. Since all the models considered in this letter do not take the presence of $\Lambda(1520)$ into account, only the region below 170 MeV/c is considered in the comparison. The blue bands show results obtained using CATS with a Coulomb potential only. The remaining curves include, on top of the Coulomb attraction, different descriptions of the $\overline{\mathrm{K}}\mathrm{N}$ strong interaction. The light blue bands show the result obtained using the chiral Kyoto model calculations with approximate boundary conditions neglecting the transitions to $\Sigma\pi$ and $\Lambda\pi$ [44–48]. The red bands indicate the result obtained with the Jülich strong potential, which has recently been updated to reproduce the SIDDHARTA results [50] and includes the $\mathrm{K}^- - \overline{\mathrm{K}}^0$ mass difference, as can be seen from the presence of the cusp around $k^* = 58$ MeV/c.

The comparison between models and data shows that the inclusion of the strong interaction is not enough to reproduce the measured correlation function, in particular in the region of k^* below 100 MeV/c. This is not surprising since the models were fitted to only reproduce scattering data above threshold (providing constraints for $k^* \geq 70$ MeV/c) and the SIDDHARTA results at threshold [27]. Moreover the Kyoto calculation considered here is performed in the so-called isospin basis and hence does not take into account the mass difference among the isospin partners K^- and $\overline{\mathrm{K}}^0$. Therefore, the effect related to isospin symmetry breaking is not present in the current version of this model. This difference in mass is present

in the Jülich model and even though this introduces the expected structure at k^* = 58 MeV/c, the shape of the correlation function cannot reproduce the data points.
To further test the stability of the results, the measured $C(k^*)$ without any S_{T} cut was used. In this case the background from mini-jets and other kinetically correlated pairs has been subtracted by using a Monte Carlo simulation based on PYTHIA 8 [55], using a procedure similar to the one described in [60]. By using this method the comparison between data and models is consistent within statistical uncertainties with the one obtained using the sphericity selection.

To summarize, the momentum dependent correlations of same-charge and opposite-charge Kp pairs (($\mathrm{K}^+\mathrm{p} \oplus \mathrm{K}^-\overline{\mathrm{p}}$) and ($\mathrm{K}^-\mathrm{p} \oplus \mathrm{K}^+\overline{\mathrm{p}}$)) were measured using the two-particle correlation function in pp collisions at different collision energies. A structure around k^* = 58 MeV/c in the measured correlation function of ($\mathrm{K}^-\mathrm{p} \oplus \mathrm{K}^+\overline{\mathrm{p}}$) was observed. The significance of such a structure was evaluated by combining the results from the three analyzed datasets and by interpolating the total correlation function with a spline. By studying the variation in the slope of the derivative of such spline in the range $50 \leq k^* \leq 60$ MeV/c, the kinematic cusp was assessed at a 4.4σ level. The observed structure is consistent with the opening of the $\overline{\mathrm{K}}^0\mathrm{n}$ channel ($p_{\mathrm{lab}} \sim 89$ MeV/c), hence this measurement represents the first experimental observation of the $\overline{\mathrm{K}}^0\mathrm{n}$ ($\mathrm{K}^0\overline{\mathrm{n}}$) isospin breaking channel due to the mass difference between K^- and $\overline{\mathrm{K}}^0$. This demonstrates how the femtoscopy technique is a unique tool to study the $\overline{\mathrm{K}}\mathrm{N}$ scattering at low momenta where the traditional scattering experiments at fixed target are difficult to realize.
The measured $C(k^*)$ were compared to different interaction scenarios. The ($\mathrm{K}^+\mathrm{p} \oplus \mathrm{K}^-\overline{\mathrm{p}}$) correlation functions were proven to be sensitive to the strong interaction, since a Coulomb-only hypothesis is insufficient to describe the data. The inclusion of the strong interaction via the Jülich model results in a good description of the data within uncertainties. The ($\mathrm{K}^-\mathrm{p} \oplus \mathrm{K}^+\overline{\mathrm{p}}$) correlation functions at low k^* cannot be reproduced by the considered potentials. The data presented in this letter provide new constraints for future low-energy phenomenological QCD calculations and can be used to shed light on the nature of the $\overline{\mathrm{K}}\mathrm{N}$ interaction.

Acknowledgements

The ALICE Collaboration is grateful to Prof. Tetsuo Hyodo and Prof. Johann Haidenbauer for the valuable suggestions and discussions.

References

[1] W. E. Humphrey and R. R. Ross, "Low-Energy Interactions of K^- Mesons in Hydrogen," *Phys. Rev.* **127** (1962) 1305–1323.

[2] M. B. Watson, M. Ferro-Luzzi, and R. D. Tripp, "Analysis of Y_0^* (1520) and Determination of the Σ Parity," *Phys. Rev.* **131** (1963) 2248–2281.

[3] T. S. Mast, M. Alston-Garnjost, R. O. Bangerter, A. S. Barbaro-Galtieri, F. T. Solmitz, and R. D. Tripp, "Elastic, Charge Exchange, and Total K^-p Cross-Sections in the Momentum Range 220 MeV/c to 470 MeV/c," *Phys. Rev.* **D14** (1976) 13.

[4] R. J. Nowak *et al.*, "Charged Σ Hyperon Production by K^- Meson Interactions at Rest," *Nucl. Phys.* **B139** (1978) 61–71.

[5] J. Ciborowski *et al.*, "Kaon scattering and charged Sigma hyperon production in K^-p interactions below 300 MeV/c," *J. Phys.* **G8** (1982) 13–32.

[6] D. Hadjimichef, J. Haidenbauer, and G. Krein, "Short range repulsion and isospin dependence in the KN system," *Phys. Rev.* **C66** (2002) 055214, arXiv:nucl-th/0209026 [nucl-th].

[7] J. Gasser *et al.*, "Physics and Detectors for DAPHNE," *Frascati Phys. Series* **16** (1999) 659.

[8] R. L. Jaffe and C. L. Korpa, "The Pattern of Chiral Symmetry Breaking and the Strange Quark Content of the Proton," *Comments Nucl. Part. Phys.* **17** no. 3, (1987) 163–175.

[9] R. H. Dalitz and S. F. Tuan, "A possible resonant state in pion-hyperon scattering," *Phys. Rev. Lett.* **2** (1959) 425–428.

[10] R. H. Dalitz and S. F. Tuan, "The phenomenological description of K-nucleon reaction processes," *Annals Phys.* **10** (1960) 307–351.

[11] J. M. M. Hall, W. Kamleh, D. B. Leinweber, B. J. Menadue, B. J. Owen, A. W. Thomas, and R. D. Young, "Lattice QCD Evidence that the $\Lambda(1405)$ Resonance is an Antikaon-Nucleon Molecule," *Phys. Rev. Lett.* **114** no. 13, (2015) 132002, arXiv:1411.3402 [hep-lat].

[12] N. Kaiser, P. B. Siegel, and W. Weise, "Chiral dynamics and the low-energy kaon - nucleon interaction," *Nucl. Phys.* **A594** (1995) 325–345, arXiv:nucl-th/9505043 [nucl-th].

[13] E. Oset and A. Ramos, "Nonperturbative chiral approach to s-wave anti-K N interactions," *Nucl. Phys.* **A635** (1998) 99–120, arXiv:nucl-th/9711022 [nucl-th].

[14] J. A. Oller and U. G. Meißner, "Chiral dynamics in the presence of bound states: Kaon nucleon interactions revisited," *Phys. Lett.* **B500** (2001) 263–272, arXiv:hep-ph/0011146 [hep-ph].

[15] M. F. M. Lutz and E. E. Kolomeitsev, "Relativistic chiral SU(3) symmetry, large N(c) sum rules and meson baryon scattering," *Nucl. Phys.* **A700** (2002) 193–308, arXiv:nucl-th/0105042 [nucl-th].

[16] T. Hyodo and W. Weise, "Effective anti-K N interaction based on chiral SU(3) dynamics," *Phys. Rev.* **C77** (2008) 035204, arXiv:0712.1613 [nucl-th].

[17] Y. Kamiya, K. Miyahara, S. Ohnishi, Y. Ikeda, T. Hyodo, E. Oset, and W. Weise, "Antikaon-nucleon interaction and $\Lambda(1405)$ in chiral SU(3) dynamics," *Nucl. Phys.* **A954** (2016) 41–57, arXiv:1602.08852 [hep-ph].

[18] J. Révai, "Are the chiral based $\overline{\mathrm{K}}$N potentials really energy dependent?," *Few Body Syst.* **59** no. 4, (2018) 49, arXiv:1711.04098 [nucl-th].

[19] M. Mai and U.-G. Meißner, "Constraints on the chiral unitary $\overline{\mathrm{K}}$N from $\pi\Sigma\mathrm{K}^+$ photoproduction data," *Eur. Phys. J.* **A51** no. 3, (2015) 30, arXiv:1411.7884 [hep-ph].

[20] B. Borasoy, U. G. Meißner, and R. Nissler, "K^- p scattering length from scattering experiments," *Phys. Rev.* **C74** (2006) 055201, arXiv:hep-ph/0606108 [hep-ph].

[21] A. Cieplý and V. Krejčiřík, "Effective model for in-medium $\bar{K}N$ interactions including the $L = 1$ partial wave," *Nucl. Phys.* **A940** (2015) 311–330, arXiv:1501.06415 [nucl-th].

[22] R. J. Hemingway, "Production of $\Lambda(1405)$ in K^-p reactions at 4.2 GeV/c," *Nucl. Phys.* **B253** (1985) 742–752.

[23] O. Braun *et al.*, "New information about the Kaon-nucleon-hyperon coupling constants g(KNΣ(1197)), g(KNΣ(1385)) and g(KNΛ(1405))," *Nucl. Phys.* **B129** (1977) 1–18.

[24] D. W. Thomas, A. Engler, H. E. Fisk, and R. W. Kraemer, "Strange particle production from π^- p interactions at 1.69 GeV/c," *Nucl. Phys.* **B56** (1973) 15–45.

[25] **HADES** Collaboration, G. Agakishiev *et al.*, "Baryonic resonances close to the $\overline{K}N$ threshold: the case of Λ(1405) in pp collisions," *Phys. Rev.* **C87** (2013) 025201, arXiv:1208.0205 [nucl-ex].

[26] **CLAS** Collaboration, K. Moriya *et al.*, "Measurement of the $\Sigma\pi$ photoproduction line shapes near the Λ(1405)," *Phys. Rev.* **C87** no. 3, (2013) 035206, arXiv:1301.5000 [nucl-ex].

[27] **SIDDHARTA** Collaboration, M. Bazzi *et al.*, "A New Measurement of Kaonic Hydrogen X-rays," *Phys. Lett.* **B704** (2011) 113–117, arXiv:1105.3090 [nucl-ex].

[28] **HADES** Collaboration, G. Agakishiev *et al.*, "Partial Wave Analysis of the reaction p(3.5 GeV)+p $\rightarrow pK^+\Lambda$ to Search for the "ppK$^-$" Bound State," *Phys. Lett.* **B742** (2015) 242–248, arXiv:1410.8188 [nucl-ex].

[29] O. Vázquez Doce *et al.*, "K^- absorption on two nucleons and ppK^- bound state search in the $\Sigma^0 p$ final state," *Phys. Lett.* **B758** (2016) 134–139, arXiv:1511.04496 [nucl-ex].

[30] S. Ajimura *et al.*, ""K^-pp", a K^--Meson Nuclear Bound State, Observed in ^{3}He(K^-, Λ p) n Reactions," arXiv:1805.12275 [nucl-ex].

[31] R. Lednicky, "Correlation femtoscopy," *Nucl. Phys.* **A774** (2006) 189–198, arXiv:nucl-th/0510020 [nucl-th].

[32] M. A. Lisa, S. Pratt, R. Soltz, and U. Wiedemann, "Femtoscopy in relativistic heavy ion collisions," *Ann. Rev. Nucl. Part. Sci.* **55** (2005) 357–402, arXiv:nucl-ex/0505014 [nucl-ex].

[33] A. Kisiel, H. Zbroszczyk, and M. Szymaski, "Extracting baryon-antibaryon strong interaction potentials from p$\bar{\Lambda}$ femtoscopic correlation functions," *Phys. Rev.* **C89** no. 5, (2014) 054916, arXiv:1403.0433 [nucl-th].

[34] **STAR** Collaboration, L. Adamczyk *et al.*, "Measurement of Interaction between Antiprotons," *Nature* **527** (2015) 345–348, arXiv:1507.07158 [nucl-ex].

[35] **ALICE** Collaboration, S. Acharya *et al.*, "p-p, p-Λ and Λ-Λ correlations studied via femtoscopy in pp reactions at $\sqrt{s}$ = 7 TeV," arXiv:1805.12455 [nucl-ex].

[36] **ALICE** Collaboration, B. Abelev *et al.*, "Performance of the ALICE Experiment at the CERN LHC," *Int.J.Mod.Phys.* **A29** (2014) 1430044, arXiv:1402.4476 [nucl-ex].

[37] **ALICE** Collaboration, E. Abbas *et al.*, "Performance of the ALICE VZERO system," *JINST* **8** (2013) P10016, arXiv:1306.3130 [nucl-ex].

[38] **ALICE** Collaboration, K. Aamodt *et al.*, "Alignment of the ALICE Inner Tracking System with cosmic-ray tracks," *JINST* **5** (2010) P03003, arXiv:1001.0502 [physics.ins-det].

[39] J. Alme, Y. Andres, H. Appelshäuser, S. Bablok, N. Bialas, *et al.*, "The ALICE TPC, a large 3-dimensional tracking device with fast readout for ultra-high multiplicity events," *Nucl.Instrum.Meth.* **A622** (2010) 316–367, arXiv:1001.1950 [physics.ins-det].

[40] A. Akindinov *et al.*, "Performance of the ALICE Time-Of-Flight detector at the LHC," *Eur. Phys. J. Plus* **128** (2013) 44.

[41] **ALICE** Collaboration, S. Acharya *et al.*, "Detailed study of the ΛΛ interaction with femtoscopy in small systems," in preparation.

[42] **ALICE** Collaboration, S. Acharya *et al.*, "Event-shape and multiplicity dependence of freeze-out radii in pp collisions at $\sqrt{s} = 7$ TeV," arXiv:1901.05518 [nucl-ex].

[43] **ALICE** Collaboration, B. Abelev *et al.*, "Transverse sphericity of primary charged particles in minimum bias proton-proton collisions at $\sqrt{s} = 0.9$, 2.76 and 7 TeV," *Eur. Phys. J.* **C72** (2012) 2124, arXiv:1205.3963 [hep-ex].

[44] K. Miyahara and T. Hyodo, "Structure of $\Lambda(1405)$ and construction of $\overline{\mathrm{K}}\mathrm{N}$ local potential based on chiral SU(3) dynamics," *Phys. Rev.* **C93** no. 1, (2016) 015201, arXiv:1506.05724 [nucl-th].

[45] S. Ohnishi, W. Horiuchi, T. Hoshino, K. Miyahara, and T. Hyodo, "Few-body approach to structure of $\bar{K}$-nuclear quasi-bound states," *Phys. Rev.* **C95** no. 6, (2017) 065202, arXiv:1701.07589 [nucl-th].

[46] **ExHIC** Collaboration, S. Cho *et al.*, "Exotic Hadrons from Heavy Ion Collisions," *Prog. Part. Nucl. Phys.* **95** (2017) 279–322, arXiv:1702.00486 [nucl-th].

[47] Y. Ikeda, T. Hyodo, and W. Weise, "Improved constraints on chiral SU(3) dynamics from kaonic hydrogen," *Phys. Lett.* **B706** (2011) 63–67, arXiv:1109.3005 [nucl-th].

[48] Y. Ikeda, T. Hyodo, and W. Weise, "Chiral SU(3) theory of antikaon-nucleon interactions with improved threshold constraints," *Nucl. Phys.* **A881** (2012) 98–114, arXiv:1201.6549 [nucl-th].

[49] M. Hoffmann, J. W. Durso, K. Holinde, B. C. Pearce, and J. Speth, "Role of correlated two pion exchange in K + N scattering," *Nucl. Phys.* **A593** (1995) 341–361, arXiv:nucl-th/9504029 [nucl-th].

[50] J. Haidenbauer, "Coupled-channel effects in hadronhadron correlation functions," *Nucl. Phys.* **A981** (2019) 1–16, arXiv:1808.05049 [hep-ph].

[51] **Particle Data Group** Collaboration, M. Tanabashi *et al.*, "Review of Particle Physics," *Phys. Rev.* **D98** no. 3, (2018) 030001.

[52] G. S. Abrams and B. Sechi-Zorn, "Charge-Exchange Scattering of Low-Energy K- Mesons in Hydrogen," *Phys. Rev.* **139** (1965) B454–B457.

[53] D. L. Mihaylov, V. Mantovani Sarti, O. W. Arnold, L. Fabbietti, B. Hohlweger, and A. M. Mathis, "A femtoscopic Correlation Analysis Tool using the Schrödinger equation (CATS)," *Eur. Phys. J.* **C78** no. 5, (2018) 394, arXiv:1802.08481 [hep-ph].

[54] T. Sjostrand, S. Mrenna, and P. Z. Skands, "PYTHIA 6.4 Physics and Manual," *JHEP* **05** (2006) 026, arXiv:hep-ph/0603175 [hep-ph].

[55] T. Sjostrand, S. Mrenna, and P. Z. Skands, "A Brief Introduction to PYTHIA 8.1," *Comput. Phys. Commun.* **178** (2008) 852–867, arXiv:0710.3820 [hep-ph].

[56] R. Brun, F. Carminati, and S. Giani, "GEANT Detector Description and Simulation Tool," *Program Library Long Write-up W5013* (1994) .

[57] **GEANT4** Collaboration, S. Agostinelli *et al.*, "GEANT4: A Simulation toolkit," *Nucl. Instrum. Meth.* **A506** (2003) 250–303.

[58] J. Haidenbauer, G. Krein, U.-G. Meißner, and L. Tolos, "DN interaction from meson exchange," *Eur. Phys. J.* **A47** (2011) 18, arXiv:1008.3794 [nucl-th].

[59] **ALICE** Collaboration, J. Adam *et al.*, "One-dimensional pion, kaon, and proton femtoscopy in Pb-Pb collisions at $\sqrt{s_{\mathrm{NN}}}$ = 2.76 TeV," *Phys. Rev.* **C92** no. 5, (2015) 054908, arXiv:1506.07884 [nucl-ex].

[60] **ALICE** Collaboration, S. Acharya *et al.*, "Measuring $\mathrm{K}^0_{\mathrm{S}}\mathrm{K}^{\pm}$ interactions using pp collisions at $\sqrt{s} = 7$ TeV," *Phys. Lett.* **B790** (2019) 22, arXiv:1809.07899 [nucl-ex].

A The ALICE Collaboration